Phenomenological modelling of the first bifurcations of spherical Couette flow

P. Manneville, L.S. Tuckerman

J. Physique **48** (1987) 1461-1469 SEPTEMBRE **1987,** PAGE 1461

Classification
Physics Abstracts
47.20 — 03.40G

Phenomenological modelling of the first bifurcations of spherical Couette flow

P. Manneville and L. S. Tuckerman (*)

Service de Physique du Solide et de Résonance Magnétique,C.E.N. Saclay, 91191 Gif-sur-Yvette Cedex, France

(Reçu le 16 février 1987, accepté le 6 mai 1987)

Résumé.-La bifurcation de l'écoulement de Couette sphérique vers l'écoulement à un rouleau de Taylor est analysée dans le cadre d'un modèle phénoménologique construit grâce à des arguments qualitatifs reposant sur des considérations de symétrie et de généricité. Les portraits de phase du système dynamique bidimensionnel correspondant sont présentés et comparés aux résultats de simulations numériques des équations de Navier-Stokes axisymétriques.

Abstract.-The bifurcation of spherical Couette flow towards the Taylor-like one-vortex flow is analysed within the framework of a phenomenological model built using qualitative arguments based on symmetry and genericity considerations. Phase portraits of the corresponding two-dimensional dynamical system are presented and compared to results of numerical simulations of the axisymmetric Navier-Stokes equations.

Introduction.

Fluid systems, or flows, which are the solutions of time-dependent, three-dimensional coupled partial differential equations, undergo transitions to qualitatively different states when some control parameter is varied. As pathways to hydrodynamic turbulence, these transitions, or bifurcations, have been a subject of renewed interest [1]. However the pre-turbulent bifurcations are interesting in their own right. Here we consider a specific example : that of spherical Couette flow, the flow between differentially rotating concentric spheres (Fig. 1).

Spherical Couette flow is a variant of the classical Taylor-Couette flow [2] in which the inner of two concentric cylinders is rotated. In the cylindrical case, when the rotation speed exceeds a critical value, the primary -strictly azimuthal- flow becomes unstable and Taylor vortices form that redistribute angular momentum between radial shells. In the spherical case, as long as curvature effects are not too strong, the first bifurcations are basically due to the same mechanism which is still expected to work in the vicinity of the equatorial plane. Unfortunately, due to the absence of any known closed-form solution for the basic state, a detailed theoretical explanation of the situation is not straightforward. To circumvent this difficulty, supplementing standard laboratory experiments, large scale numerical computations have been performed. The aim of this paper is to show that the empirical knowledge gathered in that way can be readily organized within the framework of dissipative dynamical systems theory [3].

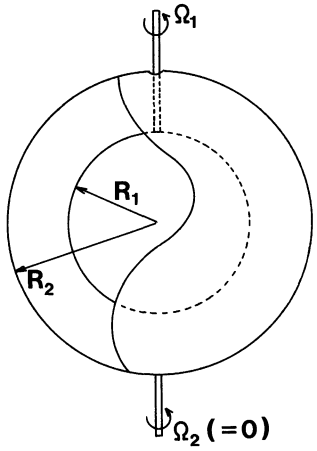

Fig.1.-Geometry of spherical Couette flow.

(*) Present address : Department of Physics, University of Texas, Austin, TX 78712, U.S.A.

After a brief survey of known results (§ 1), we build a simple Landau-like phenomenological model and show that it yields a description of the situation consistent with these results (§ 2). In the final section we present numerical simulations conducted and interpreted so as to support the dynamical systems approach.

1. Survey of previous studies.

The complete problem can be specified by a geometrical parameter, the gap :

$$\sigma = (R_2\text{-}R_1)/R_1$$

where R_1, R_2 are the inner and outer radii, and a dynamical parameter, the Reynolds number :

$$Re = \Omega_1 R_1^2/\nu$$

which measures the nondimensionalized rotation speed of the inner sphere Ω_1 (the outer sphere is assumed at rest, $\Omega_2 = 0$). ν is the kinematic viscosity of the fluid. The state of the flow is generally specified by the value of the torque Γ exerted on the outer sphere in order to keep it at rest. The bifurcation diagram is then usually drawn in the plane (Re,Γ) at given σ.

In the limit of vanishing shear, close to thermodynamic equilibrium, the flow pattern can be decomposed into i) an azimuthal component which corresponds to the simple Couette solution between infinite cylinders and ii) a small meridional correction driven by Ekman pumping which makes the complete analytical description intractable. Indeed, close to each pole the system can be viewed as a fluid layer confined between two planes approximating the two spheres. Centrifugal forces thus expel the fluid out from the pole along the rotating surface. Flow lines of this meridional velocity component close to form a pair of large-scale (pole to equator), weak vortices (see Fig. 2a below). The size of Taylor-like vortices is expected to be of the order of the gap width. Since no such small-scale vortices appear, this regime is called the zero-vortex flow (state **0**). In addition, the conventional Taylor instability is expected only when the gap parameter is small so that the basic flow in the equatorial region is sufficiently similar to that between infinite cylinders. Experimentally, this is indeed the case [4].

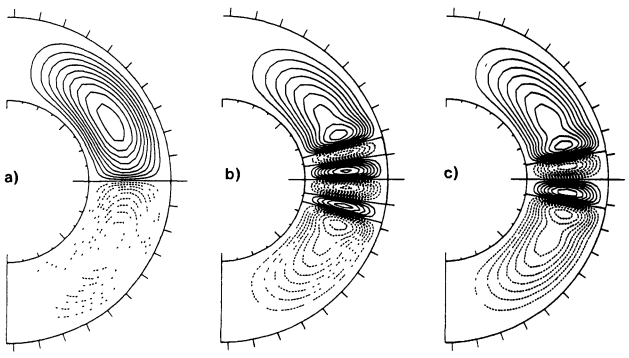

Fig.2.-Numerically obtained meridional steamlines of observed steady states : a) zero-vortex flow, b) two-vortex flow, c) one-vortex flow.

Results to be discussed below will be confined to $\sigma = 0.18$ for which a detailed picture has been obtained from laboratory experiments [5] as well as from computational studies, either numerical simulations of the full time-dependent problem which closely mimics laboratory experiments [6,7] or a direct search for solutions of the time-independent equations [8]. In contrast with the first approach, the second one can yield all steady states but no direct information on transitions between them.

At moderate Reynolds numbers, typically for $Re < 800$, laboratory experiments have shown the existence of several steady states characterized by their number of Taylor-like vortices, either zero, one, or two. In figures 2a,b,c we show the streamlines characterizing the meridional flow for each of these three states. The streamlines are obtained numerically, using the program described in reference [7] and in section 3 below. (To emphasize important features, the gap has been widened on the figures). State **0** (Fig. 2a) naturally defines the thermodynamic branch. The two-vortex flow (state **2**, Fig. 2b) has two vortices above and two vortices below the equatorial plane, the radial flow outwards in that plane. The one-vortex flow (state **1**, Fig. 2c) has one vortex in each hemisphere and the radial flow inwards in the equatorial plane. All these states are axisymmetric (as well as reflection symmetric in the equatorial plane).

The situation is complicated by the fact that the state reached by the flow depends on its history, especially on the transient acceleration of the inner sphere from rest to its final rotation rate, and on the kind of perturbations permitted by the experimental set-up or the numerical scheme. For example, both figures 2b and 2c were obtained for $Re = 900$, by using different acceleration histories [7]. A global picture of the dependence of the flow state on Re is given in figure 3a, which displays the torque Γ of zero-, one-, and two-vortex states (solid, short-dashed, and long-dashed lines, respectively) as a function of the Reynolds number Re.

The **0**-curve is seen to convert to a **2**-curve at $Re = 740$. As clearly shown by the numerical study [7], this **0-2**-transition is in fact an imperfect supercritical bifurcation, *i.e.* results from a strong nonlinear resonance of the unstable classical Taylor mode with a background modulated by the meridional velocity component. The unstable mode sets in by means of pinches in the meridional flow that act as precursors of Taylor vortices.

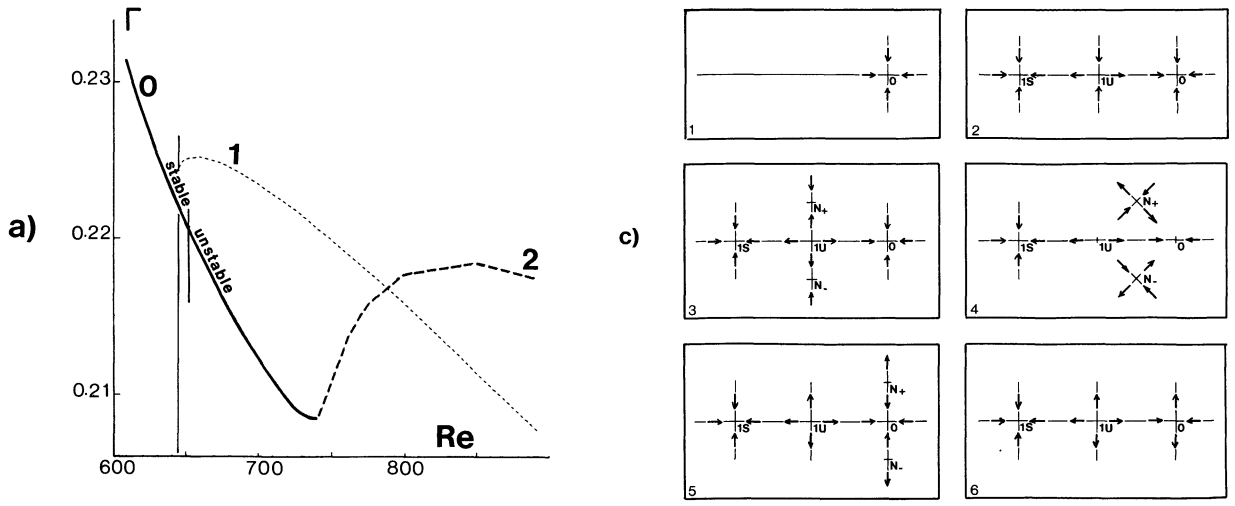

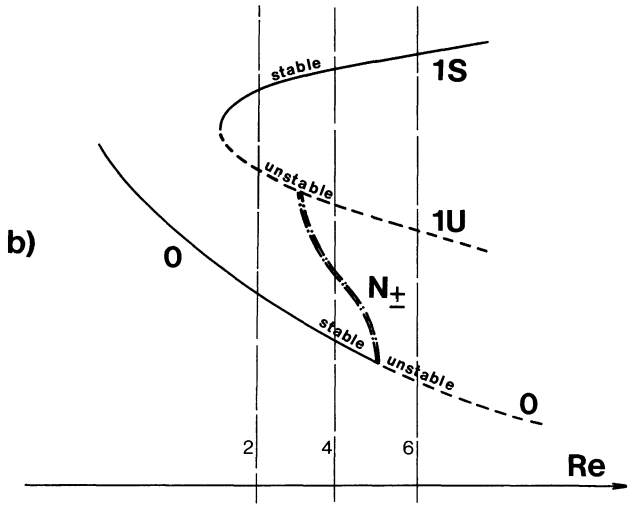

Fig.3.-Summary of previous results : a) bifurcation diagram from numerical simulations of Tuckerman [7] in agreement with laboratory experiments of Wimmer [5] : the thermodynamic branch connects the state **0** (solid line) to the state **2** (long-dashed line) while state **1** (short-dashed line) belong to a disconnected branch. State **0** is stable up to $Re = 651$. Transition to state **2** takes place only if the inner sphere is accelerated sufficiently quickly, otherwise state **1** is obtained. The crossing of branches **1** and **2** has no physical meaning : it is simply an artifact of the representation. b) schematic bifurcation diagram from Schrauf's results [8*b*,*c*] : at the turning point a branch of unstable one-vortex states appears in addition to the branch of stable states. The branch of asymmetric states, **N** connects the branches of states **0** and **1U**. Vertical lines refer to situations depicted in figures 5, 7, and 8. c) interpretation of figure 3b above in terms of phase portraits on a two-dimensional manifold parametrized by the (real) amplitudes of symmetric (*S*) and antisymmetric (*A*) perturbation to the basic flow.

A stability analysis [7] shows that between $Re = 651$ and 775, the steady states belonging to the **0-2**-curve just described are linearly unstable to an infinitesimal perturbation that has a real growth rate (no oscillatory behaviour). The spatial structure of the corresponding eigenvector is antisymmetric with respect to the equatorial plane (Fig. 4). Close to the bifurcation point, the bifurcated state computed by Schrauf [8*b*,*c*] (denoted **N** in the following) is asymmetric since it results from the combination of a small antisymmetric component proportional to this unstable wavevector and of the symmetric primary flow contribution. The initial problem being symmetric, the symmetry breaking leads in fact to one of two equivalent states, $\mathbf{N}_+$ and $\mathbf{N}_-$, which differ by the sign of their antisymmetric part. The bifurcation at $Re = 651$ turns out to be subcritical so that these states are unstable.

Disconnected from the **0-2**-curve, the **1**-curve ends abruptly at $Re = 645$. It is not possible for state **1** to branch from nothing. The endpoint must be a turning point where two companion states branch, one stable and the other unstable (saddle-node bifurcation). Only the stable state (previously **1** but more precisely **1S** in the following) can be observed in experiments or simulations. The unstable state (**1U**) can be obtained only by direct search of steady states [8]. In addition to the expected unstable state **1U**, this direct search has shown the existence of a continuous new branch of asymmetric states which connect the point where state **0** becomes unstable (subcritical bifurcation of states **N** quoted above) to a point on the **1U**-branch where the bifurcation is supercritical. The state **1U** is then doubly unstable, with respect to a symmetric eigenvector, as expected for a standard saddle-node bifurcation, but also with respect to an antisymmetric eigenvector.

Aside from the **0-2**-transition we have the complete bifurcation diagram [8*b*,*c*] involving states **0**, **1S**, **1U**, and **N** as given in figure 3b. As it stands, it

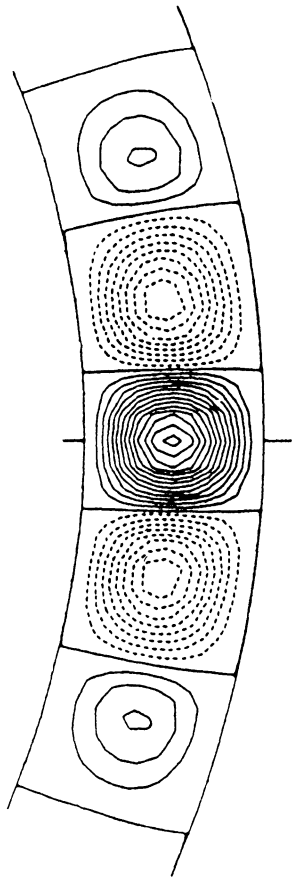

Fig.4.-Numerically obtained meridional streamlines of the unstable eigenvector of state **0**.

accounts for all known experimental results, and in particular for the fact that i) the transition from state **0** to state **1S** involves an asymmetric transient and ii) state **2** can be observed only when the acceleration of the inner sphere is sufficiently large (the antisymmetric instability of the primary state which triggers the transition from state **0** to state **1** has no time to develop). We shall now illustrate the use of dynamical systems theory in the interpretation of this simplified diagram.

2. The phenomenological model.

Systems governed by partial differential equations involve a phase space of a functional nature. However out of the formally infinite set of degrees of freedom only a finite and small subset is relevant, that of near-marginal modes. These relevant modes are called "central". Their dynamics takes place on a "center manifold" [3] obtained by an adiabatic elimination of the strongly stable modes which are slaved to them. Usually only the local structure of the center manifold close to fixed points can be obtained by perturbative methods, the global structure remaining unknown. Fortunately, in many cases of interest, such as the present one, the system does not escape to remote regions of the phase space where "weird" features of the center manifold would be important, e.g. if a direct transition to turbulence were to take place. Then one can neglect stable modes and restrict the description of the dynamical system to an evolution law for points in a low-dimensional Euclidian space locally approximating the center manifold. Moreover this evolution law can be viewed as composed of the first terms of a Taylor expansion of the actual dynamics, i.e. polynomials. Symmetry properties impose relations between the coefficients of the different terms. These coefficients can, in principle, be determined as a function of the control parameters. On the other hand, the phenomenological approach leaves them completely free, except possibly for general inequalities and supplementary assumptions mainly designed to avoid spurious difficulties in the analysis.

One should therefore obtain a good description of this region of parameter space in terms of a two-dimensional system of real variables. Let S be associated with the amplitude of that part of the flow which is reflection-symmetric about the equator, and let A represent the antisymmetric part of the flow. Then the dynamics in the S-A phase plane can be represented at various values of Re by the diagrams in figure 3c where the diagrams labelled 2, 4, and 6 refer to the Re-values drawn in figure 3b. Let us now build the simplest explicit model which yields such a sequence of phase portraits.

The saddle-node bifurcation from **0** to the pair of states **1S** and **1U** can be described by the simple differential equation :

$$\frac{dS}{dt} = a + bS - S^3. \tag{1}$$

Due to the symmetry of the primitive equations, antisymmetric perturbations can occur equivalently with either sign. The most general two-dimensional system with at most cubic nonlinearities and the required symmetry property reads :

$$\frac{dS}{dt} = (a + a' A^2) + (b - b' A^2) S - S^3 = F_S(S, A) \tag{2a}$$

$$\frac{dA}{dt} = (c + 2a'' S - b'' S^2) A - A^3 = F_A(S, A) \tag{2b}$$

This system defines a gradient flow when :

$$\frac{\partial F_S}{\partial A} = \frac{\partial F_A}{\partial S} \quad \text{i.e.} \quad a' = a'' \quad \text{and} \quad b' = b'' \tag{3}$$

then one has :

$$\frac{dS}{dt} = -\frac{\partial G(S, A)}{\partial S}$$

$$\frac{dA}{dt} = -\frac{\partial G(S, A)}{\partial A}$$

with :

$$G(S, A) = -aS - a' A^2 S - bS^2/2 - cA^2/2 + \\ + S^4/4 + b' A^2 S^2/2 + A^4/4 \tag{4}$$

Though the primitive equations have no variational structure, assumption (3) seems reasonable in view of the relaxational behaviour of the hydrodynamic fields. In order to avoid having sets of initial conditions escaping to infinity, one must take $b' > -1$, a simple situation corresponding to $b' = 1$ which we adopt in the following.

Steady states are given by :

$$0 = (a + a' A^2) + (b - A^2) S - S^3 \qquad (5a)$$

$$0 = (c + 2 a' S - S^2 - A^2) A. \qquad (5b)$$

The stability properties of these fixed points are deduced from the second derivatives of the potential :

$$\frac{\partial^2 G}{\partial S^2} = -(b - A^2) + 3 S^2 \qquad (6a)$$

$$\frac{\partial^2 G}{\partial A^2} = -(c + 2 a' S - S^2) + 3 A^2 \qquad (6b)$$

$$\frac{\partial^2 G}{\partial S \, \partial A} = -2(a' - S) A. \qquad (6c)$$

Stability is obtained when the quadratic form defined on these quantities evaluated at a fixed point is definite and positive.

Solutions of equation (5b) are either $A = 0$ which allows us to recover the purely symmetric problem (1) or possibly other non trivial solutions :

$$A^2 = c + 2 a' S - S^2 \qquad (7)$$

when the right hand side is positive. Let us first consider the symmetric solutions which are the steady states of equation (1).

Defining :

$$D = 4 b^3 - 27 a^2$$

then this equation has one steady state as long as $D < 0$ and three in the opposite case. The saddle-node bifurcation occurs precisely at $D = 0$.

At the fixed points corresponding to these solutions the second derivatives of the potential (6) assume simpler forms which make the stability analysis trivial :

$$\frac{\partial^2 G}{\partial S^2} = -b + 3 S^2,$$

$$\frac{\partial^2 G}{\partial A^2} = -c - 2 a' S + S^2 \quad \text{and} \quad \frac{\partial^2 G}{\partial A \, \partial S} = 0.$$

The fixed points remain stable against antisymmetric fluctuations as long as equation (7) has no real solutions. In the direction of symmetric perturbations one gets the expected unstable solution between the two stable solutions. The corresponding phase portrait is displayed in figure 5 where it can be seen that the stable manifold of the saddle point separates the basin of attraction of the two stable nodes.

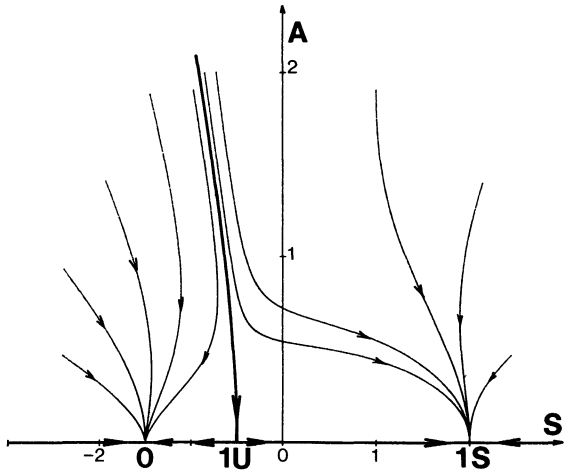

Fig.5.-Phase portrait of system (2) with $a = 3/2$, $b = 13/4$ and $c = 0$, corresponding to situation (2) in figure 3b : the stable manifold of the unstable state **1U** separates the basin of attraction of the stable states **0** and **1S**. We show only the upper half of the phase portrait (which can be completed by reflecting about the S-axis).

Here we do not wish to discuss all the possible kinds of behaviour permitted by the most general dynamical system (2) but simply show how the left part of the diagram in figure 3b is contained in the gradient restriction to (2). Consequently we shall specify the problem a little more and choose a set of parameters which will allow us to reproduce all experimental and numerical results easily.

Assuming :

$$a = 3/2 \quad \text{and} \quad b = 13/4$$

one gets symmetric fixed points at $A = 0$ and

$$S = 2, \quad \text{stable}, \quad \text{state } \mathbf{1S},$$

$$S = -1/2, \quad \text{unstable}, \quad \text{state } \mathbf{1U},$$

$$S = -3/2, \quad \text{stable}, \quad \text{state } \mathbf{0}.$$

Nontrivial states without symmetry are given by the intersection of the curve given by (7) and that given by (5a), i.e. :

$$A^2 = (a + bS - S^3) / (S - a')$$

For simplicity we assume $a' = 0$ so that the only remaining control parameter is c (codimension-one scenario). Then this last equation reads :

$$A^2 = S^2 + b + a/S$$

The graphical solution is presented in figure 6. There can be a physical nontrivial solution only for $1/4 < c < 9/4$:

$$S = 6/(4c - 13) \quad \text{and} \quad A = \sqrt{(c - S^2)}.$$

For $c < 1/4$, all three fixed points are stable against antisymmetric perturbations. At $c = 1/4$, state **1U** bifurcates and a new fixed point appears

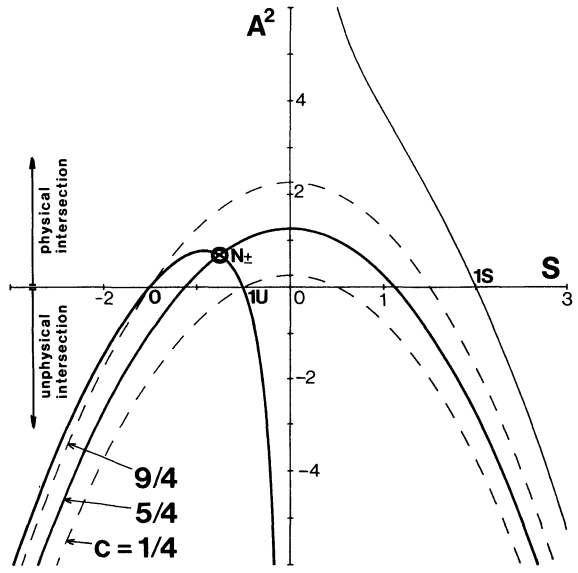

Fig.6.-Graphical solution for asymmetric states **N**. The square of the amplitude of the antisymmetric part is given by the intersection of the two curves. This intersection is physically meaningful for $1/4 < c < 9/4$. $c < 1/4$ corresponds to situation (2) with phase portrait as in figure 5 and $9/4 < c$ to situation (6) in figure 8.

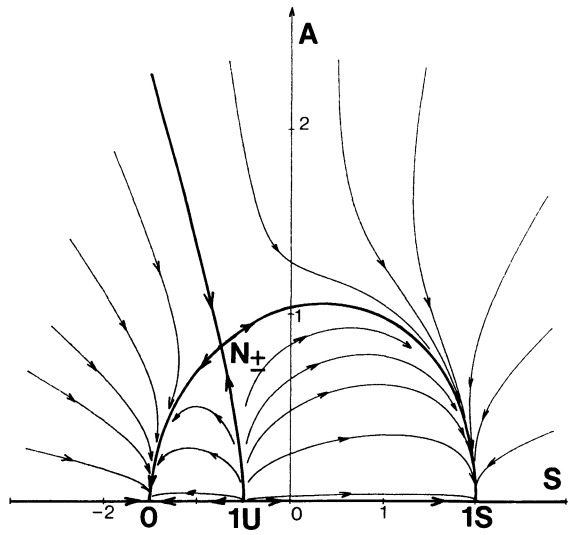

Fig.7.-Phase portrait for $c = 5/4$, displaying all relevant states, in particular state **N** with its stable and unstable manifolds (situation (4) in Fig. 3b).

which is seen to be a saddle. The phase portrait for $c = 5/4$ is given in figure 7. The stable and unstable manifolds of this new fixed point have been drawn together with some trajectories. At $c = 9/4$ this fixed point collides with the node at $(-3/2,0)$ — state **0** — which becomes a saddle. The phase portrait for $c = 11/4$ is given in figure 8. All the trajectories end at the only remaining fixed point (2,0) — state **1S** — in particular the unstable manifold of state **0**. Trajectories issuing from the vicinity of point $(-1/2,0)$ — state **1U** — depart linearly from this

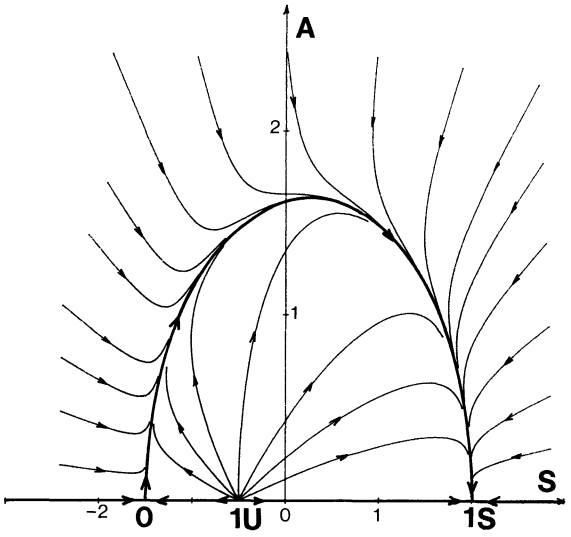

Fig.8.-Phase portrait for $c = 11/4$, merging of states **0** and **N**. State **0** is now a saddle unstable to antisymmetric perturbations, and its unstable manifold directly joins state **1S**.

point. This is due to an accidental degeneracy of the two positive eigenvalues of the linear stability problem for this specific value of c.

Clearly this scenario is generic : it holds for open sets of parameter values around those we have chosen. A qualitatively similar picture is expected for different but sufficiently close values of the parameters a', a'', b, b', b'' even in the nonpotential case. A further step would be to account for the transition to the two-vortex state, which would require starting with a polynomial in S of higher order and a new small parameter controlling the imperfection. It would not be difficult to adapt the approach to different physical situations, such as a different gap values, rotation of the outer sphere, or else Taylor vortices in cylinders of finite height [9], etc. and to interpret the relevant bifurcation diagrams in the same manner.

3. Dynamical systems approach *versus* simulations.

The aim of the numerical study presented in this section is limited to a check of the structure of the (reduced) phase space depicted in figure 7 and in particular, an analysis of the vicinity of state **1U**. When trying to apply the dynamical systems approach to laboratory or simulation results, one has to face the problem of phase space reconstruction. The experimental study of the transition to turbulence has promoted the method of delays on the time series of physical observables [10]. In numerical simulations, the complete phase space, or at least a good approximation of it, is directly available. However since the actual dynamics takes place on a much reduced manifold, one can legitimately ask for

a simplified representation in terms of a small set of relevant variables which describe qualitative features of the phenomena, in this case symmetry properties.

Here we need a quantitative counterpart to components S and A introduced in the preceding section. It turns out that the size of the vortices is a good measure of the symmetric part of the flow (see Fig. 9). Its only drawback is that the final decay towards state **0** cannot be reproduced using it since the boundary between the opposite circulating vortices merges with the equatorial plane slightly before state **0** is actually reached as will be seen in figure 13 (the remainder of the transition is spent forming the pinches mentioned previously). The amount of antisymmetry can be measured in several ways. One can take, for example, the energy contained in the antisymmetric part of the flow or any difference between two quantities defined in each hemisphere. Here we have chosen the former solution. Using these coordinates, the experimentally determined dynamics on the center manifold happened to present fewer spurious trajectory crossings than do other pairs of variables tried in the region of interest.

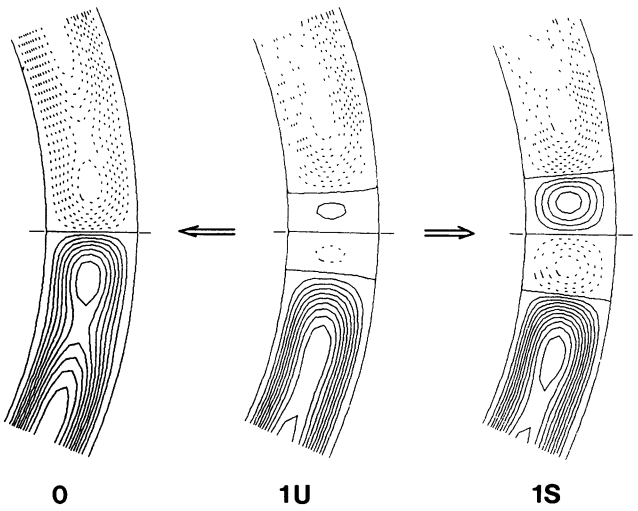

Fig.9.-Meridional streamlines of states **0**, **1U** and **1S** for Re between 645 and 651, situation (4) in figure 3b. (State **1U** is derived by projecting and adjusting Schrauf's data [8*d*]). Note that vortex sizes are ordered in a convenient way (*i.e.* **1U** is intermediate between **0** and **1S**) to serve as a measure of the symmetrical part of the flow.

The algorithm used to solve the axisymmetric time dependent Navier-Stokes equations in a spherical layer has been described elsewhere [7]. A pseudo-spectral method [11] is employed. The radial dependence is represented by an expansion in terms of Chebychev polynomials (typically 16 polynomials) while a sine series is used for the angular dependence (with up to 128 or even 256 terms). The code was optimized in order to take advantage of vectorized features of the CRAY-1 computer.

As in laboratory experiments, unstable steady states cannot be obtained directly in simulations since all trajectories are expelled along unstable manifolds. On the other hand direct search of steady states can give all steady states, stable or unstable. As an initial condition we have taken the approximation to state **1U** given to us by G.Schrauf who used a finite difference code [8]. However after projection on the basis of Chebychev polynomials, this approximation was no longer a steady state but evolved rapidly towards state **1S**. A trial-and-error approach using the difference between two successive states as an estimate of the evolution velocity allowed us to go backwards closer and closer to state **1U**.

Once the (quasi-)steady state was obtained, by a modified algorithm equivalent to the classical power method, we could extract the largest eigenvalues and eigenvectors corresponding to the most unstable infinitesimal perturbations : one symmetric **WS** ($\lambda = 0.25$) and one antisymmetric **WA** ($\lambda = 0.019$). The meridional streamlines of these eigenvectors are given in figure 10. Using them as unit vectors in the space tangent to the center manifold at the unstable node **1U** one expects trajectories as sketched in figure 11. The difference with the behaviour of trajectories in the vicinity of **1U** is not essential : a better choice of coefficients in the model would lead to a correct ordering of eigenvalues and restore the agreement. What is worth searching for is the stable manifold of state **N** which serves as a boundary between the basins of attraction of states **0** and **1S**. Since from figure 11 the most sensitive direction is that of eigenvector **WA**, we have chosen to add a

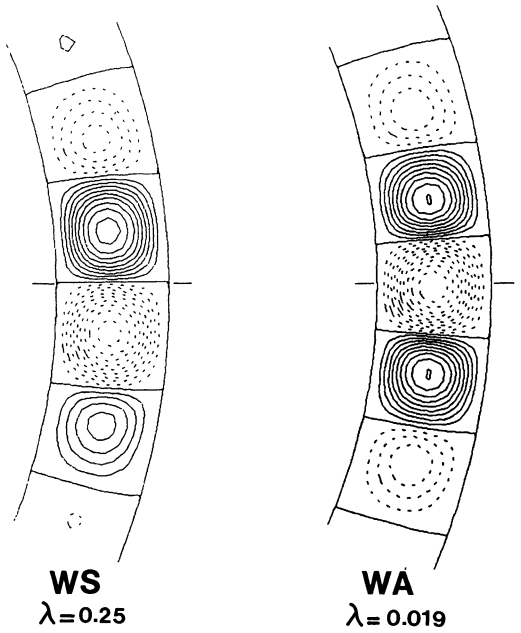

Fig.10.-Meridional streamlines of eigenvectors **WS** and **WA** of state **1U**.

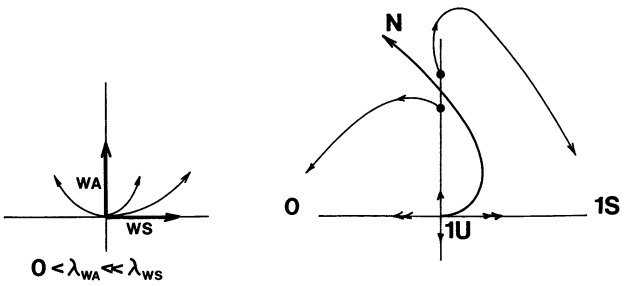

Fig.11.- a) Sketch of the phase portrait close to a node unstable in two directions with different eigenvalues, one large and one small. b) The stable manifold of state **N** must reach state **1U** as an ordinary trajectory, *i.e.* not necessarily tangent to the direction **WA**. Initial conditions chosen in the direction of eigenvector **WA** on either side of this special trajectory must belong to the basin of attraction of states **0** and **1S**.

fraction of this eigenvector to state **1U**. Time series of the total torque corresponding to four trajectories are displayed in figure 12. Two of them go to state **0** and the others to state **1S**, which is straightforwardly interpreted in figure 11b. In particular close to state **1U**, the stable manifold of state **N** must behave as an ordinary trajectory ; it has no reason to follow the direction of eigenvector **WA**. The boundary of the basins of attraction can be obtained by interpolation. Using physical observables described above as coordinates one gets the picture in figure 13 which is a

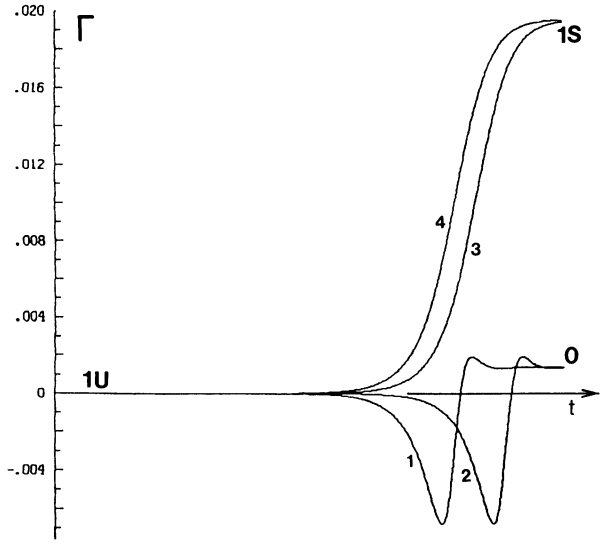

Fig.12.-Time series of the total torque for initial conditions **1U** plus a component proportional to eigenvector **WA** measured by the antisymmetric energy. Trajectories (1) and (2) (antisymmetric energy equal to 4.0×10^{-5} and 4.125×10^{-5} respectively) belong to the basin of attraction of state **0** and trajectories (3) and (4) (with 4.25×10^{-5} and 4.85×10^{-5}) to the basin of **1S**. Note that in both cases the final torque is larger than the initial one. This ordering makes the torque unsuitable for the quantifying variable **S**.

reasonably good perspective view of the actual phase portrait in the neighborhood considered. Indeed further from the unstable point, some unknown nonlinear change of coordinate is required to recover the picture in figure 7 but one can easily identify the aborted approach to the saddle point **N**.

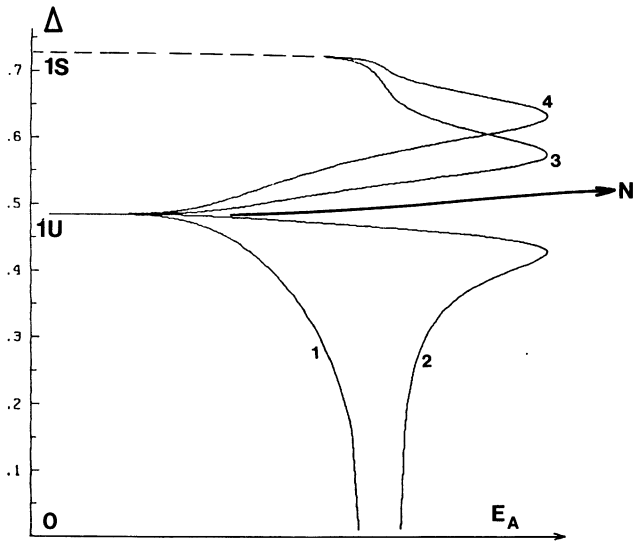

Fig.13.-Experimental phase portrait using the width of the vortices (Δ) and the antisymmetric energy (E_A) as variables (same initial conditions as for Fig.12.- For the trajectories leading to state **1S**, crossings are a minor artifact of the representation chosen, and obtaining a complete decay would require a longer simulation (dotted prolongation). The analogous decay to state **0** is truncated due to the fact that the width of vortices drops to zero before the end of the transition. State **N** could be approached more closely along its stable manifold by adjusting the amplitude of the component along eigenvector **WA**.

Of course, neither the phenomenological analysis developed in section 2 nor the numerical simulations above have been fully exploited. However we hope to have shown the virtues of the dynamical systems approach, where bifurcation theory works as a useful organizing tool. Physical situations where a combination of empirical results and dynamical system methods could prove valuable are numerous. An analytical approach from first principles is often intractable in practice, as here, when there is no known exact solution for the basic state, or when bifurcation analysis from perturbation theory is still unsufficiently developed, (an example of the latter would be the oscillatory square to roll transition in convection [12]). Extensions are not difficult to imagine, even to time-dependent cases that would require the use of Poincaré sections. They would be probably difficult to work out but the kind of phenomenological modelling used here seems a promising way to get a thorough understanding of complicated nonlinear pre-turbulent problems.

Acknowledgments.

The authors would like to thank G.Schrauf who kindly communicated his steady solution for state 1U and the Centre de Calcul Vectoriel pour la Recherche (Palaiseau, France) for a CPU time allocation on its Cray-1S (project n° 2721).

References

[1] See for example : *Hydrodynamic instabilities and the transition to turbulence* 2nd Edition, H.L. Swinney and J.P. Gollub (Eds.) (Springer, Berlin), 1986.

[2] Di Prima R.C., and Swinney H.L. in reference [1] above.

[3] Guckenheimer J., and Holmes J., : *Nonlinear Oscillations, Dynamical Systems, and Bifurcation of Vector Fields* (Springer, Berlin), 1983.

[4] Belyaev Y.N., Monakov A.A., and Yavorskaya I.M., *Fluid Dyn.* **2** (1978) 162.

[5] Wimmer M., J. *Fluid Mech.* **78** (1976) 317.

[6] Bartels F., J. *Fluid Mech.* **119** (1982) 1.

[7] a) Tuckerman L.S., *Formation of Taylor vortices in spherical Couette flow*, PhD Thesis, MIT (1983) and b) Tuckerman L.S., and Marcus P.S. in *Ninth International Conference on Numerical Methods in Fluid Dynamics*, Soubbaramayer and Boujot (Eds) *Lect. Notes Phys.* **218** (Springer, Berlin) 1985. c) Marcus P.S. and Tuckerman L.S., *J. Fluid Mech.*, in press.

[8] a) Schrauf G., PhD Thesis, Universitat Bonn (1983), b) Schrauf G. and Krause E., in *Second IUTAM Symposium on laminar-turbulent transition* (Springer, Berlin), 1984, also : c) Schrauf G., in Fourth Taylor Vortex Flow working party, 20-22 May 1985, Universitat Karlsruhe, unpublished. d) Schrauf G., private communication.

[9] Mullin T., *J. Fluid Mech.* **121** (1982) 207.

[10] Takens F., *Lect. Notes Math.* **898** (Springer, Berlin), 1981, p.366.

[11] Gottlieb D., Orszag S.A. : *Numerical Analysis of Spectral Methods : Theory and applications* (SIAM Press, Philadelphia), 1977.

[12] Le Gal P., Pocheau A., and Croquette V., private communication and *Phys. Rev. Lett.* **54** (1985) 2501.